2

Chapter 2

2.1 Experimental Techniques Used in Dielectric and Electro Optic Measurements

In this chapter, we describe the experimental setup used in measuring (i) optical phase difference, (ii) dielectric constants $\epsilon_\perp$ and $\epsilon_\parallel$, (iii) splay and bend elastic constants as functions of temperature, using a *single sample cell*. This is possible if the nematic liquid crystal has positive dielectric anisotropy, which is the case for all the materials studied in this thesis. In this chapter, we describe the technique and present results on 4-*n*-octyloxy 4′-cyanobiphenyl (8OCB) which is used to test the setup.

2.2 Construction of Cell

First we describe the construction of the cells used in the optical, electro optical and dielectric measurements. We have used two types of liquid crystal cells depending upon the sample. The first one is used for single component samples which are chemically robust. The two sides of the cell are open, but will not affect the long term stability of samples. The second type of cell is used for two component (mixture) samples, and is fully enclosed. Both types of cells are made of two ITO coated glass plates. A circular pattern is etched on both plates to get an active area with 8mm diameter (see Fig 2.1a, Fig 2.1b). In order to get planar alignment of the sample, we have used two types of treatments. (i) The two etched plates are coated with a thin layer of polyimide and cured at 250 °C for one and half hours. Then both the plates are rubbed in a specific direction. (ii) In the other method, SiO is vacuum coated on both the plates at 32 ° grazing angle. The molecules sit in the grooves created by the rubbing on the polyimide surfaces or those formed by the shadowing effect in the SiO coated plates to give a planar or homogeneous alignment. Cells are made by placing the two plates together, ensuring that the active areas overlap (Fig 2.1c). The separation is controlled by glass-bead spacers with diameter of $\sim$8 μm, which are mixed with an epoxy glue. The cell is cured at 150 °C for one and half hours after the glue is applied at the edges of the plates. The thickness of the empty cell is measured with $\pm$1% accuracy by an interferometric technique using Ocean Optics Spectrometer.

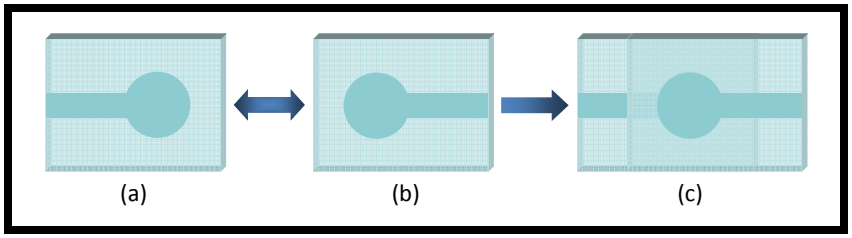

FIGURE 2.1: (a), (b) are the top views of the two plates, (c) the two are glued together to form the liquid crystal cell.

The capacitance of the empty cell is measured before filling the sample. The cell is filled with the sample by capillary suction in the isotropic phase. As the experimental runs extended for 3-4 weeks, a gradual concentration change is noticed in mixtures used with the cells exposed at two

sides. To overcome this problem, a 3rd glass plate with a central hole (for reducing unnecessary reflections) is placed on top of the upper ITO coated plate after filling the liquid crystal sample. This 3rd plate is larger in size than the top ITO coated plate. Appropriate glass strips are sealed (using epoxy glue) to completely cover the gaps between the lower ITO plate and the uppermost plate. The gap between the edges of the hole of the top plate and the upper part of the top ITO plate is also sealed. In this case, it is necessary to give the electrical connection to the top ITO plate also through the bottom ITO plate. This is ensured by etching an appropriate electrode on the bottom plate and making the electrical contact to the upper ITO plate using silver paste, which is applied outside the sealed LC cell (Figure 2.2). This "*pill-box*" (Figure 2.2) ensures that the mixture is not exposed to external atmosphere. The four sides of the external pill box are sealed by silicone glue (taking care that the glue does not come into contact with the liquid crystal sample) and maintained at room temperature for 36 hours for hardening. The cell is placed inside an Instek mk1 heater to control the temperature to 5mK accuracy. The whole system is placed on the stage of a polarizing microscope (ORTHOLUX, II POL-BK).

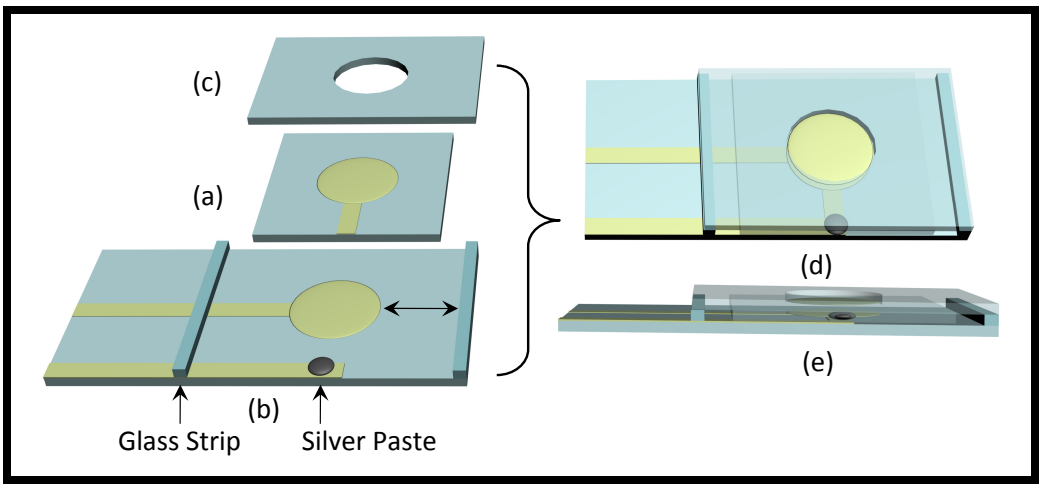

Figure 2.2: (a) and (b) are SiO coated top and bottom plates respectively, (c) top plate with a central hole (d) perspective view of the pill-boxed enclosed LC cell and (e) side view of the LC cell. $\longleftrightarrow$ indicates the alignment direction of director.

2.3 Temperature Calibration

A thermistor is used to measure and to control the sample temperature. The temperature T can be determined by measuring its resistance $R\,(\Omega)$ which follows the following relation, according to mk1 manual:

$$T = -273.15 + \frac{10^4}{A_0 + A_1 \ln\, R + A_2 \ln^3\, R} \tag{2.1}$$

where A_0, A_1 and A_2 are the coefficients of the thermistor, which are different for different thermistors. To determine these coefficients we need at least three calibration temperatures at which the corresponding resistances are measured. We have used a few liquid crystalline samples whose Isotropic-Nematic transition temperatures (T_{NI}) are known (see Table 2.1).

Liquid Crystal Compounds	**T_{NI}(°C)**
8CB (4′-n-octyl-4-cyanobiphenyl)	40.0
CP6B (p-cyanophenyl p-n-hexylbenzoate)	47.5
CP7B (p-cyanophenyl p-n-heptylbenzoate)	56.5
MPPCC (p-methoxyphenyl trans-4-pentylcyclohexane carboxylate)	71.1
6OCB (4-hexyloxy 4′-cyanobiphenyl)	75
8OCB (4-*n*-octyloxy 4′ -cyanobiphenyl)	79.8
[7(CN)5] (2-cyano 4-heptylphenyl 4′-pentyl-4-biphenyl carboxylate)	103.2
CE8 (4-(2′-methyl butyl) phenyl 4′-n-octylbiphenyl-4-carboxylate)	140.7
PCPPB (trans-4-propylcyclohexyl-4-(4-propylphenyl) benzoate)	186

Table 2.1: List of liquid crystal compounds and the isotropic-nematic transition temperatures T_{NI} (in °C)

The samples are taken between two glass slides, placed inside the heater and observed under crossed polarizers. First the samples are heated to the isotropic phase and then slowly cooled ($\sim$2 °C/minute). At T_{NI} the thermistor resistances are measured. The Temperature-Resistance graph is shown in Figure 2.3.

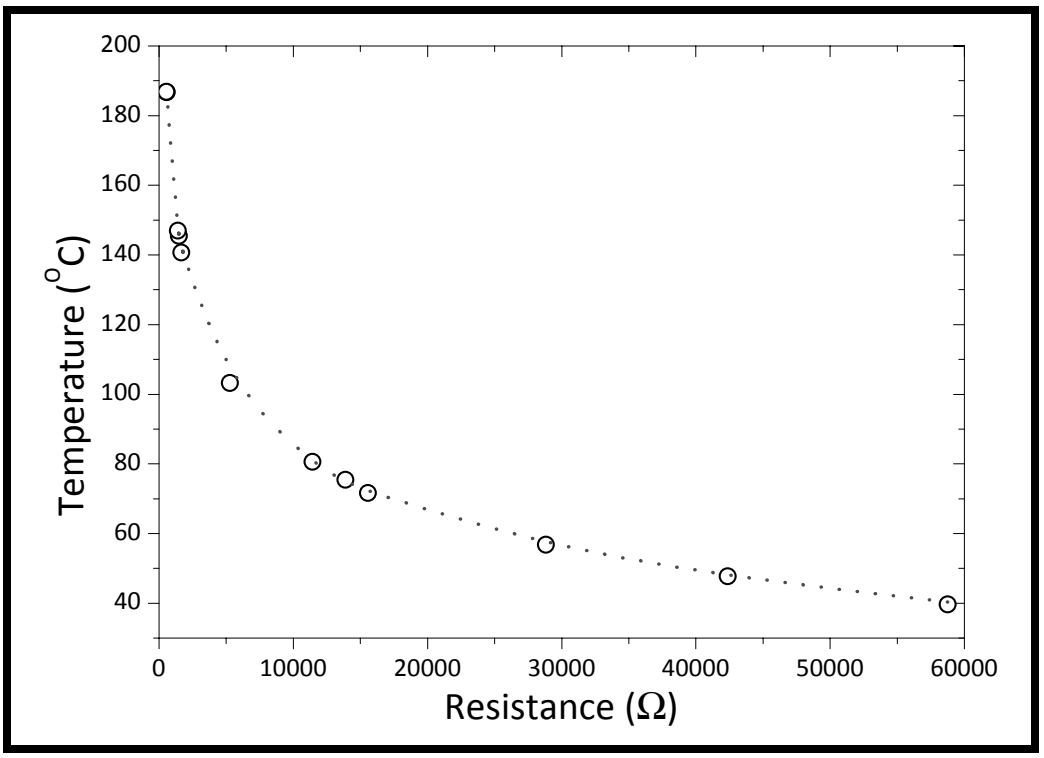

Figure 2.3: Temperature Resistance graph

The open circles are measured points and the continuous line is fitted using Equation (2.1). From fitting we get the values of the three coefficients, $A_0 = 8.29762$, $A_1 = 2.12088$ and $A_2 = 0.00023$.

2.4 Experimental Setup for Optical and Dielectric Measurements

A He-Ne laser (wavelength $\lambda = 6328$ Å.) beam is passed through a linear polarizer. It is then split into two parallel beams using a beam splitter. The two beams are chopped at two different frequencies in the ratio 11:18 (with mutually exclusive Fourier components) by a dual frequency chopper made by Perkin Elmer (model no. 198A). One of the beams (reference) is directly routed to the photo-diode. The other beam passes through another polarizer, the sample cell and an analyzer (crossed with respect to polarizer) before entering the same photo-diode. The

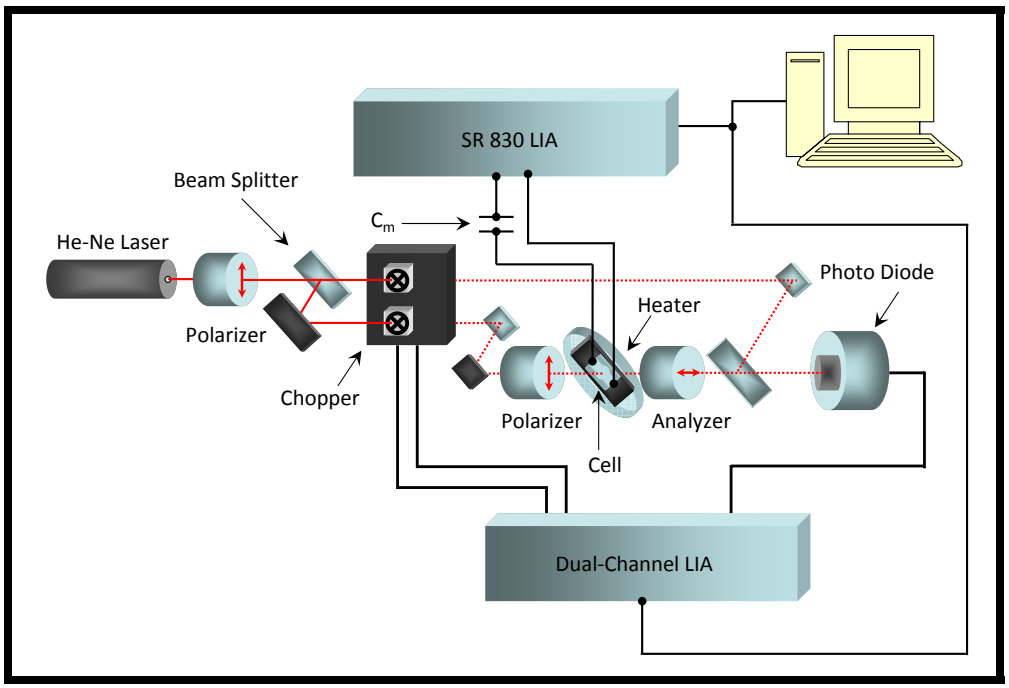

FIGURE 2.4: Schematic diagram of the electro optical setup

photo-diode is connected to a dual-channel lock-in amplifier made by Perkin Elmer (model no. 7265A). This enables us to measure the intensity of both the beams simultaneously. We use the ratio of the sample beam intensity to the reference beam intensity in further analysis to take care of any source intensity fluctuations. Another lock-in amplifier (Stanford Research System, model no. SR830) is connected to the cell in series with a fixed capacitance ($C_m = 1\mu$F) to measure the impedance of the cell (see Fig 2.4 and Figure 2.6)

2.5 Optical Measurements :

The transmitted intensity of light emerging from the homogeneously aligned sample is given by,

$$I_{Tr} = I_0 \frac{\sin^2 2\psi}{2} (1 - \cos \delta\Phi) \tag{2.2}$$

where I_0 is the intensity of the incident (linearly polarized) beam, ψ is the angle made by the optic axis with the polarizer and the phase difference

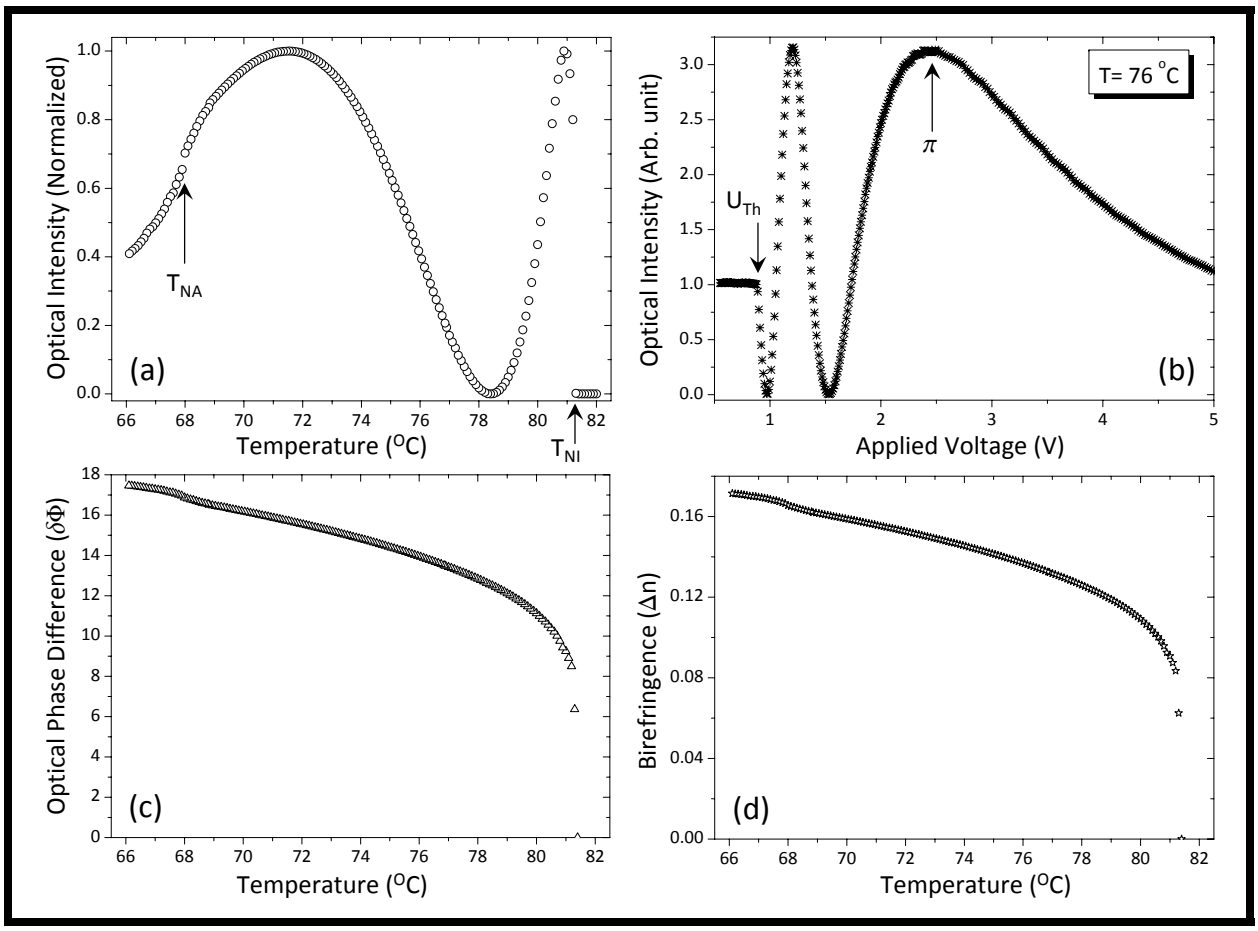

Figure 2.5: (a) Normalized transmitted intensity as a function of temperature in 8OCB. (b) Variation of optical intensity with applied voltage at 76 °C. The calculated temperature dependences of (c) the phase difference (in radians) and (d) the birefringence of 8OCB.

$$\delta\Phi = \frac{2\pi}{\lambda}\,\Delta n\, L. \tag{2.3}$$

$\Delta n = (n_e - n_o)$ where n_e and n_o are the extraordinary and ordinary refractive indices of the liquid crystal medium respectively. L is the sample thickness. The angle ψ is fixed at 45 ° to get the maximum sensitivity. The optical intensity is an oscillatory function of $\delta\Phi$ (Figure 2.5a). The absolute phase difference $\delta\Phi$ is found by applying a high electric field to the nematic sample with *positive* dielectric anisotropy. At a fixed temperature (in the nematic phase), at high applied voltages, the phase difference tends to zero (Figure 2.5b). The electric field is then slowly decreased and the absolute phase difference is calculated by counting the number of maxima and

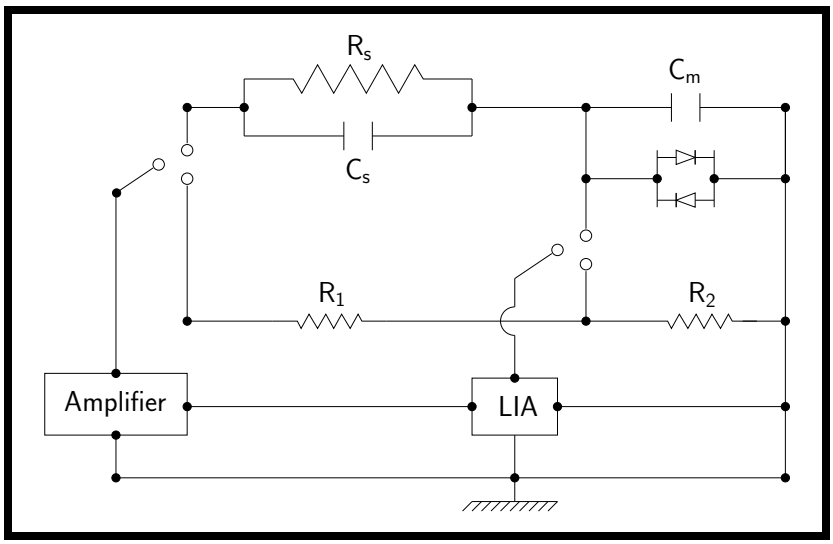

FIGURE 2.6: Schematic diagram of the electrical circuit with the RC equivalent of the liquid crystal cell

minima. The birefringence is obtained from the absolute value of $\delta\Phi$ (Figure 2.5c & d).

2.6 Impedance Analysis of the Sample

The liquid crystal samples are not free of ionic impurities and exhibit finite resistances. The equivalent electrical circuit of a liquid crystal cell can hence be considered to be a capacitance (C_s) and resistance (R_s) in parallel (see Figure 2.6). A fixed capacitor, C_m ($= 1\mu$F) is connected in series with the LC cell. C_m is very large compared to the cell capacitance ($\sim$nF). An ac signal at a frequency $\sim$5.64 kHz from the lock-in amplifier (Stanford Research System, model no. SR830) is connected to a voltage amplifier. The output of the amplifier is connected to one of the two branches, either a potential divider or the LC cell in series with C_m, by a manual double pole double throw (DPDT) switch. The potential divider is made of two resistors $R_1 = 1\text{M}\Omega$ and $R_2 = 100\Omega$ connected in series. The potential divider circuit is used to measure the output phase and amplitude of the *amplified* voltage. The amplitude and phase of the voltage developed across C_m are measured by the same lock-in amplifier (LIA). If C_m is large, a large part of the voltage drops across the cell and only a small voltage is measured by LIA. To protect the LIA from accidental high currents, for example if the cell gets shorted, two similar zener diodes

(breakdown voltage ∼2.6 V) with their opposite polarities interconnected as shown in Figure 2.6, and connected across the input of the LIA. Using impedance analysis, we measure the capacitance C_s and resistance R_s of the sample.

The impedance of the LC cell is given by,

$$Z_C = R_s \frac{1 - j\,\omega\, C_s\, R_s}{1 + \omega^2\, C_s^2\, R_s^2} \tag{2.4}$$

where $\omega = 2\pi f$ and f is the frequency of the applied voltage and $j = \sqrt{-1}$. The total impedance of the circuit is given by,

$$Z_T = \frac{\omega R_s C_m - j[1 + \omega^2\, R_s^2\, C_s(C_m + C_s)]}{\omega\, C_m(1 + \omega^2\, C_s^2\, R_s^2)} \tag{2.5}$$

Let an ac *input* voltage $V = V_0\, e^{j(\omega t + \phi_0)}$ be applied to the circuit, where ϕ_0 is the phase. The total current I_T is given by,

$$I_T = \frac{V_0\, e^{j(\omega t+\phi_0)}}{Z_T} = \frac{V_0\, e^{j(\omega t+\phi_0)}\, \omega\, C_m(1 + \omega^2\, C_s^2\, R_s^2)}{\omega\, R_s\, C_m - j[1 + \omega^2\, R_s^2\, C_s(C_m + C_s)]} \tag{2.6}$$

The voltage drop across C_m which is measured by the lock-in amplifier is given by,

$$V_m\, e^{j(\omega t+\phi_m)} = I_T\, Z_m = I_T\, \frac{1}{j\,\omega\, C_m} \tag{2.7}$$

where V_m and ϕ_m are the amplitude and phase of the measured voltage. Comparing real and imaginary parts we get,

$$V_m \cos(\omega t + \phi_m) = V_0 \frac{[1 + \omega^2\, C_s(C_m + C_s)R_s^2] \cos(\omega t + \phi_0) + \omega\, C_m R_s\, \sin(\omega t + \phi_0)}{1 + \omega^2\, (C_m + C_s)^2\, R_s^2} \tag{2.8}$$

and,

$$V_m \sin(\omega t + \phi_m) = V_0 \frac{[1 + \omega^2\, C_s(C_m + C_s)R_s^2] \sin(\omega t + \phi_0) - \omega\, C_m R_s\, \cos(\omega t + \phi_0)}{1 + \omega^2\, (C_m + C_s)^2\, R_s^2} \tag{2.9}$$

Solving equations (2.8) and (2.9) we get,

$$\boxed{Cs = \frac{C_m\, V_m[V_0\, \cos(\phi_m - \phi_0) - V_m]}{V_0^2 + V_m^2 - 2\, V_0\, V_m\, \cos(\phi_m - \phi_0)}} \tag{2.10}$$

and,

$$\boxed{Rs = \frac{V_0^2 + V_m^2 - 2\, V_0\, V_m\, \cos(\phi_m - \phi_0)}{\omega\, V_0\, C_m\, V_m\, \sin(\phi_m - \phi_0)}} \tag{2.11}$$

The dielectric constant of the sample is the ratio of the filled (C_s) cell capacitance and empty (C_0) cell capacitance i.e. C_s/C_0. The conductivity of the sample, $\sigma = L/(R_s\, A)$, where A is the effective area and L is the thickness of the cell. To measure the stray capacitance added to the circuit by the coaxial cable used to connect the LIA to the cell, we have used a standard capacitor and resistor connected in parallel in place of LC cell and repeated the above analysis. The stray capacitance is found to be $\sim$6 pF. The accuracies of the measured capacitance and resistance are estimated to be $\sim$5% and $\sim$10% respectively.

2.7 Measurements of Both Principal Dielectric Constants of Nematic Samples

As described above, an ac signal of frequency 5641 Hz from the lock-in amplifier (Stanford Research System, model no. SR830) is applied to the cell and the amplitude and phase of the voltage developed across C_m is measured using the same lock-in amplifier. From the impedance analysis (using equation 2.10 and 2.11), the capacitance and resistance of the cell are measured. The dielectric constant of the liquid crystal sample is the ratio of the capacitance of filled cell to that of the empty cell. If a voltage well below the Fréedericksz threshold voltage[1] is applied to the planar liquid crystal cell, the director remains perpendicular to the electric field. This measurement gives the perpendicular dielectric constant ($\epsilon_\perp$).

The maximum output of SR830 is 5V. This is not sufficient to get a strong deformation of the

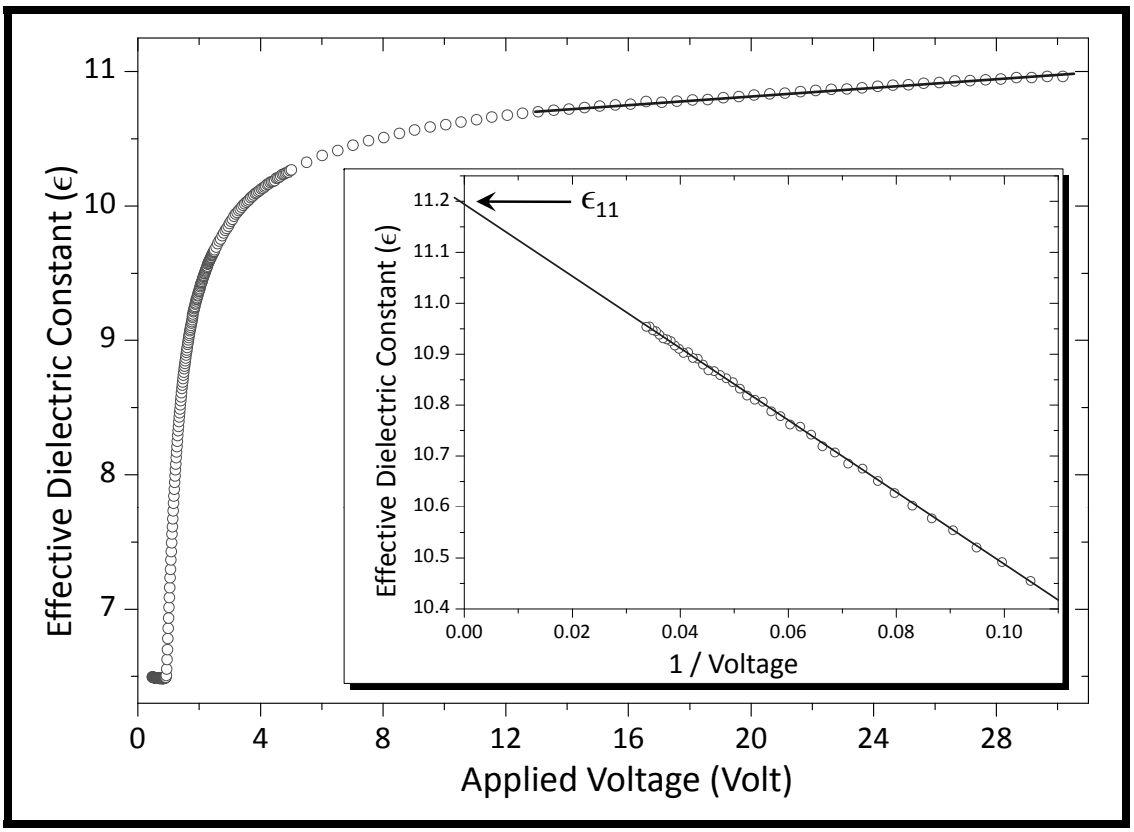

Figure 2.7: Variation of effective dielectric constant as a function of voltage. Inset: extrapolation of the linear part of higher voltage data to $1/V = 0$ to determine $\epsilon_{\parallel}$

director field which enables a measurement of $\epsilon_{\parallel}$, the dielectric constant parallel to the director. An external voltage amplifier with a gain of 6 is used to attain higher voltages. The applied voltage is varied from 0.2V to 30V and the effective dielectric constant is measured as a function of the voltage (Figure 2.7). The dielectric constant remains unaltered up to the Fréedericksz threshold, then increases rapidly and at higher voltages the rate of increase comes down and the experimental curve tends to saturate. The linear part of dielectric constant at high voltages is plotted against $1/V$ and fitted to a straight line. The dielectric constant corresponding to $\epsilon_{\parallel}$ is determined by extrapolating to $1/V = 0$.

2.8 Theoretical Analysis Needed for Measuring K_{11} and K_{33} Using Fréedericksz Transition Technique

The simplest way of measuring the elastic constant is to apply a field which is orthogonal to the director of a well aligned sample. Above a threshold field the director orientation distorts and it is called the Fréedericksz transition[20]. There are three possible geometries for measuring the three elastic constants (see Figure 1.10 of Chapter 1). In this thesis, we will be using only one geometry. All our materials have positive dielectric anisotropy, and we use homogeneously aligned samples. The threshold voltage to distort the director field will be a measure of the splay elastic constant, as we shall describe later. An analysis of the director distortion at higher fields will be used to determine the ratio of splay to bend elastic constants. Though we will measure both optical intensity and capacitance as functions of voltage, we will use only optical data to measure the bend elastic constant, as it is collected over a small area of the sample with better thickness uniformity compared to the full area of the electrodes.

The liquid crystal is enclosed between two conducting glass plates with a gap L. Let the plates lie in the x-y plane and the director **n** be parallel to the x-axis. The dielectric anisotropy of the liquid crystal is positive. If an electric field **E** is applied along the z-axis, the dielectric energy is lowered by a tilting of the director. In the most general case, the director is anchored on both the surfaces with a pretilt angle $\phi(0) = \phi(L)$. The tilt angle $\phi(z)$ is a function of the coordinate z and reaches a maximum value ϕ_m at $z = L/2$. The gradient of the tilt angle of the director increases the elastic energy. There are four possible boundary conditions depending upon the anchoring energy and the pretilt at the surface of the cell.

(i) *Zero pretilt angle and infinite surface anchoring energy* : The angle at the surface is independent of electric field ($\phi(0) = \phi(L) = \phi_0 = 0$).

(ii) *Zero pretilt but finite anchoring energy* : The angle at the surface is a function of the electric field, $\phi_0 = \phi(U)$

(iii) *Non-zero pretilt but infinite anchoring energy* : The angle at the surface is fixed ($\phi_t =$ pretilt angle) and independent of electric field.

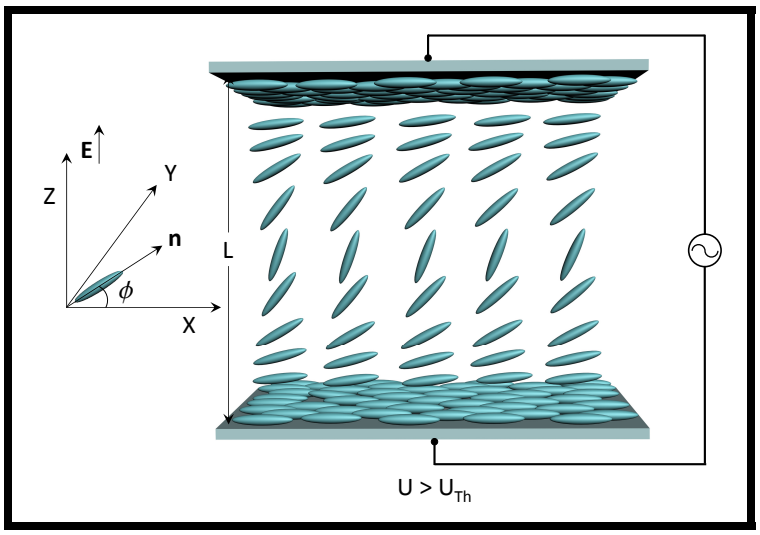

Figure 2.8: The distribution of director field under an applied electric field. The glass plates are shown in 2D while the director profile in the interior of the cell is shown only in one plane.

(iv) *Both non-zero pretilt and finite anchoring energy* : With an applied electric field the angle at the surface deviates. This deviation increases with the field.

Only with the first boundary condition, a perfect Fréedericksz threshold voltage can be obtained. The director and electric field vary with the position z and we write,

$$\mathbf{n} = (\cos\phi(z), 0, \sin\phi(z)) \tag{2.12}$$

$$\mathbf{E} = (0, 0, E(z)) \tag{2.13}$$

The total free energy per unit area of the cell is given by[21],

$$G = \frac{1}{2}\int_o^L \Big\{(K_{11}\cos^2\phi + K_{33}\sin^2\phi)\left(\frac{d\phi}{dz}\right)^2 - \mathbf{E}\,.\,\mathbf{D}\Big\}dz + 2f_s(\phi_0) \tag{2.14}$$

where the two terms of the integrand are due to elastic and dielectric energy densities, the sum of which is denoted by g later in the analysis. The other term is the Rapini Papoular[19] form of the surface energy given by,

$$f_s(\phi_0) = \frac{1}{2} W_s \sin^2(\phi_0 - \phi_t) \quad \text{at} \quad z = 0, L \tag{2.15}$$

with ϕ_0 is the actual *tilt* angle at the surface. We assume that there are no free ions in the liquid crystal and **E** satisfies the Maxwell's equations [21], $\boldsymbol{\nabla}\cdot\mathbf{D} = 0$ and $\boldsymbol{\nabla}\times\mathbf{E} = 0$. This means that, the z component (D_z) of the displacement vector **D** is a constant. D_z can be written in terms of voltage $U\left(= \int_0^L E(z)dz\right)$,

$$D_z = \frac{\epsilon_0 U}{\int_0^L (\epsilon_\parallel \sin^2\phi + \epsilon_\perp \cos^2\phi)^{-1} dz} \tag{2.16}$$

The dielectric energy per unit area,

$$\begin{aligned} -\frac{1}{2}\int_0^L \mathbf{E}\,.\,\mathbf{D}\, dz &= -\frac{1}{2} D_z \int_0^L E(z)dz \\ &= -\frac{1}{2} \frac{\epsilon_0 U^2}{\int_0^L (\epsilon_\parallel \sin^2\phi + \epsilon_\perp \cos^2\phi)^{-1} dz} \end{aligned} \tag{2.17}$$

Equation (2.14) can be expressed as,

$$\begin{aligned} G &= \frac{1}{2}\int_0^L \left[\left(K_{11}\cos^2\phi + K_{33}\sin^2\phi\right) \left(\frac{d\phi}{dz}\right)^2 \right] dz \\ &\quad -\frac{1}{2}\epsilon_0 U^2 \left\{ \int_0^L \frac{dz}{(\epsilon_\parallel \sin^2\phi + \epsilon_\perp \cos^2\phi)} \right\}^{-1} + 2 f_s(\phi_0) \end{aligned} \tag{2.18}$$

The minimization of the bulk free energy leads to the Euler-Lagrange equation[22, 23]

$$\frac{d}{dz}\left(\frac{\partial g}{\partial \phi'}\right) - \frac{\partial g}{\partial \phi} = 0 \tag{2.19}$$

where, g (integrand part) is the bulk free energy density and $\phi' = d\phi/dz$. The Euler-Lagrange equation yields the following relation :

$$\frac{d}{dz}\left[\left(K_{11}\cos^2\phi + K_{33}\sin^2\phi\right) \left(\frac{d\phi}{dz}\right)^2 - \frac{D_z^2}{\epsilon_0(\epsilon_\parallel \sin^2\phi + \epsilon_\perp \cos^2\phi)} \right] = 0 \tag{2.20}$$

Using the boundary condition, $\phi(0) = \phi(L) = \phi_0$ (assuming pretilt angle) and the maximum distorted angle of the director field at the center $\phi(L/2) = \phi_m$ (see Figure 2.8), where $d\phi/dz = 0$ we get,

$$\frac{d\phi}{dz} = D_z \sqrt{\frac{\gamma}{\epsilon_0 \epsilon_\perp K_{11}}} \left[\frac{\sin^2 \phi_m - \sin^2 \phi}{(1 + \gamma \sin^2 \phi_m)(1 + \kappa \sin^2 \phi)(1 + \gamma \sin^2 \phi)} \right]^{\frac{1}{2}} \tag{2.21}$$

where $\kappa = (K_{33} - K_{11})/K_{11}$ and $\gamma = (\epsilon_\parallel - \epsilon_\perp)/\epsilon_\perp$

We integrate over half the cell thickness. This is adequate because of symmetry of the distortion.

$$D_z = \frac{2}{L} \sqrt{\frac{\epsilon_0 \epsilon_\perp K_{11}}{\gamma}} \sqrt{1 + \gamma \sin^2 \phi_m} \int_{\phi_0}^{\phi_m} \left[\frac{(1 + \kappa \sin^2 \phi)(1 + \gamma \sin^2 \phi)}{\sin^2 \phi_m - \sin^2 \phi} \right]^{\frac{1}{2}} d\phi \tag{2.22}$$

Substituting $\sin \phi = \sin \phi_m \sin \psi$ and using the value of D_z we get the following expression for the applied voltage :

$$\boxed{\frac{U}{U_{Th}} = \frac{2}{\pi} \sqrt{1 + \gamma \sin^2 \phi_m} \int_{\Theta}^{\frac{\pi}{2}} \left[\frac{(1 + \kappa \sin^2 \phi_m \sin^2 \psi)}{(1 + \gamma \sin^2 \phi_m \sin^2 \psi)(1 - \sin^2 \phi_m \sin^2 \psi)} \right]^{\frac{1}{2}} d\psi} \tag{2.23}$$

where, $\Theta = \sin^{-1}\big(\sin \phi_0 / \sin \phi_m\big)$ and

$$\boxed{U_{Th} = \pi \sqrt{\frac{K_{11}}{\epsilon_0 \epsilon_\perp \gamma}}} \tag{2.24}$$

is the Fréedericksz threshold voltage. If pretilt angle $\phi_0 \neq 0$, $\phi_m = \phi_0$ even when $U = 0$ and we do not get any threshold voltage[24, 25] and the tilt angle ϕ starts to increase from ϕ_0 as the

field is increased from 0. If $\phi_0 = 0$, $\phi_m = 0$ when $U = 0$, and there is a Fréedericksz threshold at $U = U_{Th}$, if the anchoring energy is strong.

Now the torque balance condition at the surface is given by,

$$\left(\frac{\partial g}{\partial \phi'}\right)_{z=0,L} = \left(\frac{\partial f_s}{\partial \phi}\right)_{z=0,L} \tag{2.25}$$

where, g (integrand part) is the bulk free energy density and $\phi' = d\phi/dz$. Simplifying we get,

$$(K_{11}\cos^2\phi_0 + K_{33}\sin^2\phi_0)\left(\frac{d\phi}{dz}\right)_0 = \frac{1}{2}W_s \sin 2(\phi_0 - \phi_t) \tag{2.26}$$

where at the surface,

$$\left(\frac{d\phi}{dz}\right)_0 = D_z\sqrt{\frac{\gamma}{\epsilon_0\epsilon_\perp K_{11}}}\left[\frac{\sin^2\phi_m - \sin^2\phi_0}{(1+\gamma\sin^2\phi_m)(1+\kappa\sin^2\phi_0)(1+\gamma\sin^2\phi_0)}\right]^{\frac{1}{2}} \tag{2.27}$$

Using the value of $(d\phi/dz)_0$ at the surface and using the boundary condition $\phi' = 0$ at $z = L/2$ we get,

$$W_s = \frac{4K_{11}\,\mathbb{I}}{L\sin 2(\phi_0 - \phi_t)}\left[\frac{(1+\kappa\sin^2\phi_0)(\sin^2\phi_m - \sin^2\phi_0)}{1+\gamma\sin^2\phi_0}\right]^{\frac{1}{2}} \tag{2.28}$$

where,

$$\mathbb{I} = \int_\Theta^{\frac{\pi}{2}}\left[\frac{(1+\kappa\sin^2\phi_m\sin^2\psi)(1+\gamma\sin^2\phi_m\sin^2\psi)}{(1-\sin^2\phi_m\sin^2\psi)}\right]^{\frac{1}{2}}d\psi \tag{2.29}$$

For any applied voltage, the optical phase difference is given by,

$$\delta\Phi = \frac{2\pi}{\lambda}\int_0^L [n_{eff}(z) - n_o]dz \tag{2.30}$$

where, $n_{eff}(z) = n_e\, n_o/\sqrt{({n_e}^2\sin^2\phi + {n_o}^2\cos^2\phi)}$ is the effective extraordinary index at z. Changing the variable from z to ϕ and by using Equation (2.21) in Equation (2.30) we get,

$$\delta\Phi(U) = 2\pi\frac{n_e L}{\lambda}\left[\frac{\int_{\Theta}^{\frac{\pi}{2}}\sqrt{\frac{(1+\gamma\sin^2\phi_m\sin^2\psi)(1+\kappa\sin^2\phi_m\sin^2\psi)}{(1-\sin^2\phi_m\sin^2\psi)(1+\nu\sin^2\phi_m\sin^2\psi)}}\,d\psi}{\int_{\Theta}^{\frac{\pi}{2}}\sqrt{\frac{(1+\gamma\sin^2\phi_m\sin^2\psi)(1+\kappa\sin^2\phi_m\sin^2\psi)}{(1-\sin^2\phi_m\sin^2\psi)}}\,d\psi} - \frac{n_o}{n_e}\right] \tag{2.31}$$

where, $\nu = ({n_e}^2 - {n_0}^2)/{n_0}^2$ and $\delta\Phi$ is a function of applied voltage U. In the experiment we measure the optical phase difference as a function of applied voltage. Equations(2.23 and 2.31) are the most important equations in our analysis. For a fixed temperature the experimentally obtained optical phase difference is fitted using Equation (2.23) and (2.31) for different applied voltages by using Θ, ϕ_m and κ as adjustable parameters. The iterative fitting algorithm is written in *Mathematica* software. From this fitting we estimate that the accuracy in the values of K_{33} is $\pm 5{-}10\%$

2.9 Experimental Results and Analysis

To calibrate our setup we used the well known liquid crystal 4-*n*-octyloxy 4′-cyanobiphenyl (8OCB). Measurements of various physical properties of this material are available in the literature. In the first experimental run, an ac electric voltage (well below the Fréedericksz threshold voltage) is applied to measure ϵ_{iso} in the isotropic phase and $\epsilon_{\perp}$ in the nematic and smectic phases. The sample is cooled from the isotropic phase in small steps. The sample is equilibrated for $\sim$ 90 seconds at each temperature. Then optical and dielectric data are recorded using a computer. The data are collected down to room temperature or till the sample crystallization temperature. From this run, birefringence (Δn) and perpendicular dielectric constant ($\epsilon_{\perp}$) are measured.

In the second experimental run, the temperature is again raised above T_{NI}. The sample is cooled to a fixed temperature in the nematic phase and an ac electric voltage of 5.46 kHz frequency is applied. The voltage is increased in small steps from a value lower than the Fréedericksz threshold voltage. At each voltage the sample is allowed to stabilize for $\sim$ 20 seconds. Then simultaneously both optical and dielectric data are recorded. Extrapolating the dielectric constant to an applied

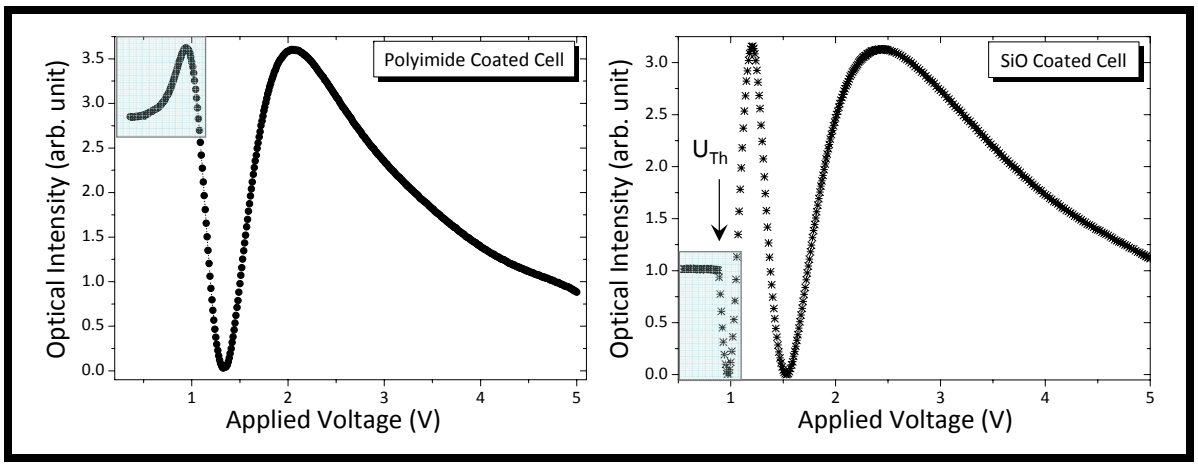

FIGURE 2.9: The tranmitted optical intensity measured in two types of cells. (a) Polyimide coated cell does not show a sharp threshold voltage, (b) SiO coated cell exhibits a sharp threshold voltage.

voltage of infinity (*ie.*, $1/\mathrm{V} = 0$), the parallel dielectric constant ($\epsilon_{\parallel}$) is obtained (see Section 2.7). From the optical data, the Fréedericksz threshold voltage is determined (see Figure 2.5b).

In polyimide coated homogeneous cells we do not get a sharp threshold voltage. The optical intensity starts varying at very low voltages and changes rapidly around the Fréedericksz voltage *ie.*, the threshold is rounded off (see Figure 2.9a). But SiO coated cells give rise to a perfect Fréedericksz threshold voltage. Upto the threshold voltage the optical intensity remains practically constant and at the threshold the optical intensity suddenly changes (see Figure 2.9b).

It is informative to compare measured phase difference of 8OCB samples in the two different types of (polyimide and SiO) cells. If ϕ_0 is assumed to be zero, the birefringence data using polyimide coated cell is about 10% lower compared to the data using SiO coated cell (see Figure 2.10a). The perpendicular dielectric constant ($\epsilon_{\perp}$) of 8OCB is also compared with these two types of coated cells. In this case $\epsilon_{\perp}$ using polyimide coated cell is larger than that from the SiO coated cell (see Figure 2.10b). These differences arise because of pretilt angle ϕ_0 (at the surface). The polyimide coated rubbed cells have pretilt angle[25], while SiO coated cells have essentially zero pretilt. The pretilt of polyimide coated cell can be calculated using the following equation,

$$n_{eff} = \frac{n_e\, n_o}{\sqrt{({n_e}^2 \sin^2\phi_0 + {n_o}^2 \cos^2\phi_0)}} \tag{2.32}$$

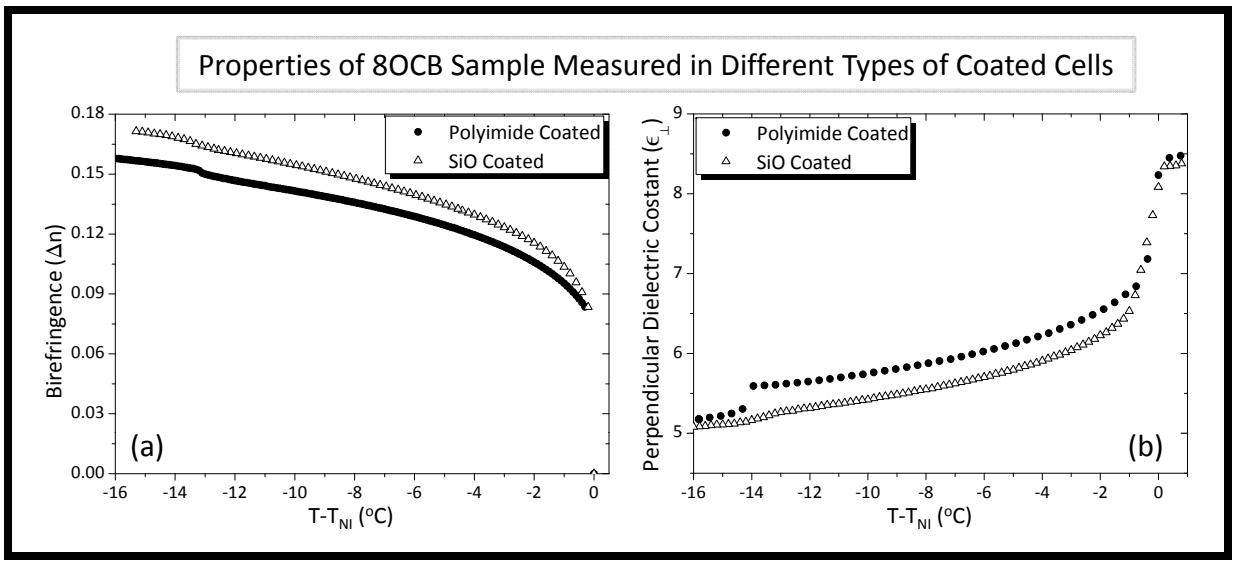

Figure 2.10: (a) birefringence and (b) $\epsilon_\perp$ measured using cells coated with polyimide and silicon monoxide (SiO).

where n_{eff} is the effective extraordinary refractive index due to pretilt angle ϕ_0 at the surface which fixes $\phi = \phi_0$ in the entire cell. On the other hand, n_o is not affected by the pretilt. From the two measured data on polyimide and SiO coated cells, the pretilt angle of polyimide cell is estimated to have a value of $\sim 14^\circ$. The large pretilt angle is useful in display devices, but it is not useful for measuring physical properties. Hereafter wards in all the subsequent measurements, we present data measured using only SiO coated cells.

We have compared our 8OCB birefringence data using SiO coated cell with those of Lim *et al.* [26]. They also used SiO coated cells and our results show a good agreement with their data (see Figure 2.11). In both cases, the slope of the curve changes close to the nematic-smectic transition temperature. The dielectric anisotropy of 8OCB is compared with the data of Bradshaw *et al.* [27]. Our data are somewhat higher, and the difference increases close to T_{NI} (Figure 2.12).

Using the SiO coated cell we get a sharp Fréedericksz threshold voltage (Figure 2.9) which is used to determine the splay elastic constant (see Equation (2.24))[28]. Above the threshold voltage, the director tilts depending on the field strength, and due to this tilt, the optical phase difference is decreased. The relation between the transmitted optical intensity I_{Tr} and the optical

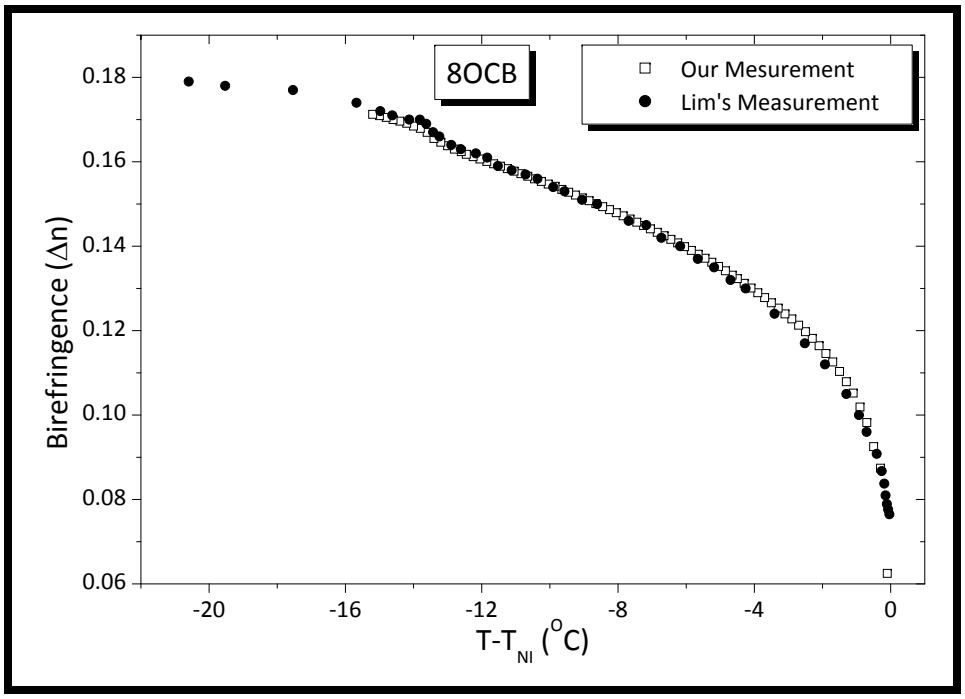

FIGURE 2.11: Measured values of birefringence of 8OCB sample. □ represent our measurements and ● represent Lim's[26] measurements.

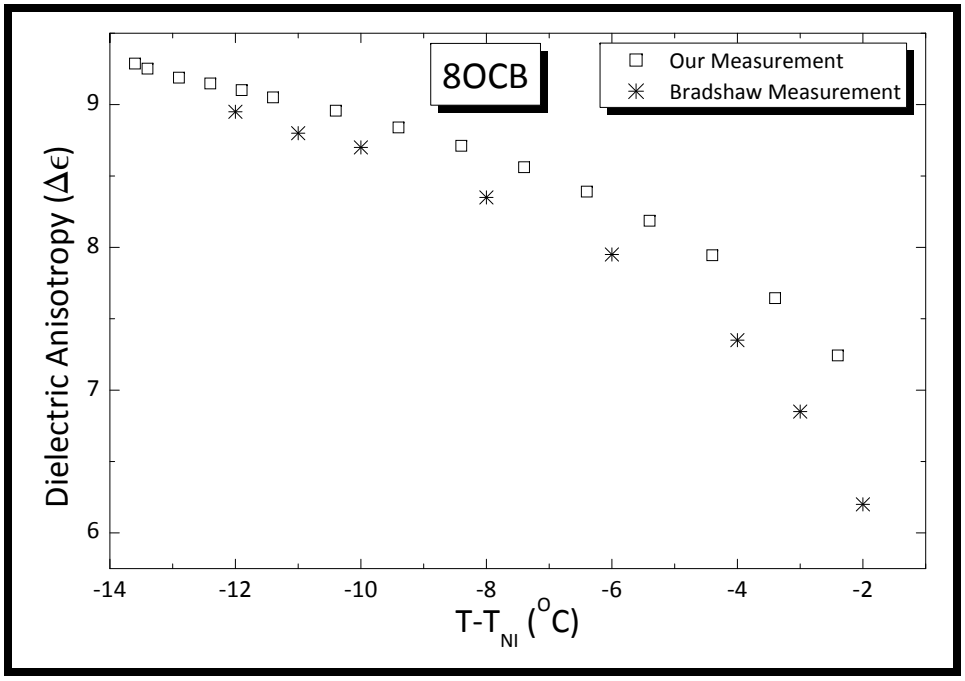

FIGURE 2.12: Measured values of dielectric anisotropy of 8OCB sample. □ represent our measurements and ⁎ represent Bradshaw's[27] measurements.

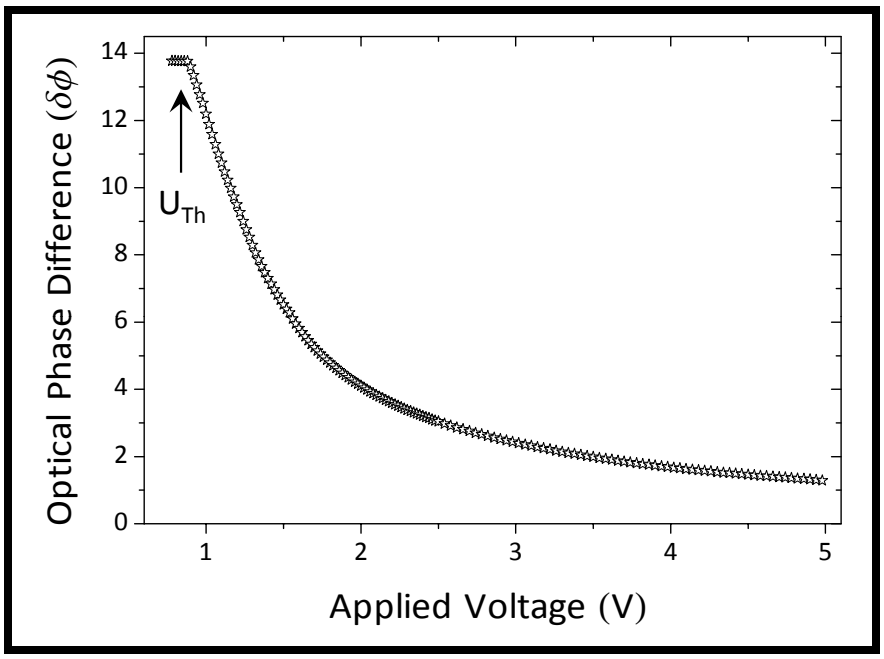

FIGURE 2.13: Optical Phase difference versus Voltage at 76°C

phase difference $\delta\Phi$ is given by,

$$I_{Tr} = \frac{I_0}{2}(1 - \cos\delta\Phi) \tag{2.33}$$

where I_0 is the intensity of the incident linearly polarized beam. The transmitted optical intensity I_{Tr} is an oscillatory function of the applied voltage. I_{Tr} is normalized by using the maximum and minimum intensities in each branch. At high voltages I_{Tr} tends to zero as $\delta\Phi$ approaches zero. If the voltage is decreased from a high value, at some voltage I_{Tr} reaches a maximum which corresponds to $\delta\Phi = \pi$ radian. Using Equation (2.33) and I_{Tr}, $\delta\Phi$ is calculated for different voltages. At a fixed temperature the variation of $\delta\Phi$ against voltage is shown in Figure 2.13. This variation is fitted with the theoretical expressions Equations (2.31) and (2.23). From the best fit the bend elastic constant K_{33} is obtained.

2.10 Measurements Above U_{Th} : Fitting Procedure

To calculate the bend elastic constant we have made a non linear least square fitting of the

experimental data to the theoretical relations. The fitting algorithm is written in *Mathematica* software considered as a platform. Here we have not used any standard set of fitting method like that of Levenberg-Marquardt[29, 30]. To fit the experimental data above the Fréedericksz threshold, we need a few material parameters. These are : birefringence (Δn), ordinary refractive index (n_o) parallel ($\epsilon_\parallel$) and perpendicular ($\epsilon_\perp$) dielectric constants and splay elastic constant (K_{11}). First we choose reasonable values of κ and anchoring energy ($W_s \sim 150\times 10^{-6}$ N/m). For this value of W_s, using Equation (2.28) we generate a set of values of tilt angle of director at the surface (ϕ_0) and maximum angle of director at the center of the cell (ϕ_m). To generate the theoretical results we need to integrate an elliptic integral. This and other elliptical integrations are evaluated numerically by the *inbuilt package* of Mathematica software. Using this set of ϕ_0 and ϕ_m, the voltage U (using Equation 2.23) and optical phase difference $\delta\Phi$ (using Equation 2.31) are calculated. We have calculated for voltages upto 2.5 times of U_{Th}. Experimentally we have measured the change of optical phase difference with applied voltage (see Figure 2.13). The experimental values of applied voltages generally do not coincide with the theoretically calculated values. The experimental data is interpolated to match the theoretical values. The experimental optical phase difference is also obtained by interpolating to the new voltage values. For these voltages, we take the difference between theoretically calculated and experimentally obtained optical phase differences and calculate the mean square deviation (χ^2). Now ϕ_0, κ and W_s are varied as fit parameters to lower the value of χ^2. By finding the minimum value of χ^2, the best fit parameters ϕ_0, κ and W_s are evaluated. From κ and K_{11} we calculate the bend elastic constant K_{33}. For the SiO coated cell we get, $W_s \sim 200\times 10^{-6}$ N/m which implies a strong anchoring and the maximum pretilt angle $\phi_0 \sim 2^\circ$.

In the numerical fitting, two optical parameters are required, *viz.* the ordinary index n_o and the birefringence Δn. As we have described earlier, we have measured Δn, but not n_o. Karat has measured both ordinary (n_o) and extra-ordinary (n_e) refractive indices of 8OCB sample at $\lambda = 632.8$ nm as functions temperature[31]. Figure 2.14 shows that n_o does not depend very much on temperature and has a value close to 1.5 except near T_{NI}. This is indeed the case in most nematic liquid crystals. The variation of Δn is mainly due to that of n_e. In 8OCB within 14°C temperature the variation of n_o is $\approx$ 1%. The value of K_{33} changes only by 1.5% if this variation is separately taken into account. The optical phase difference (Equation (2.31)) is far

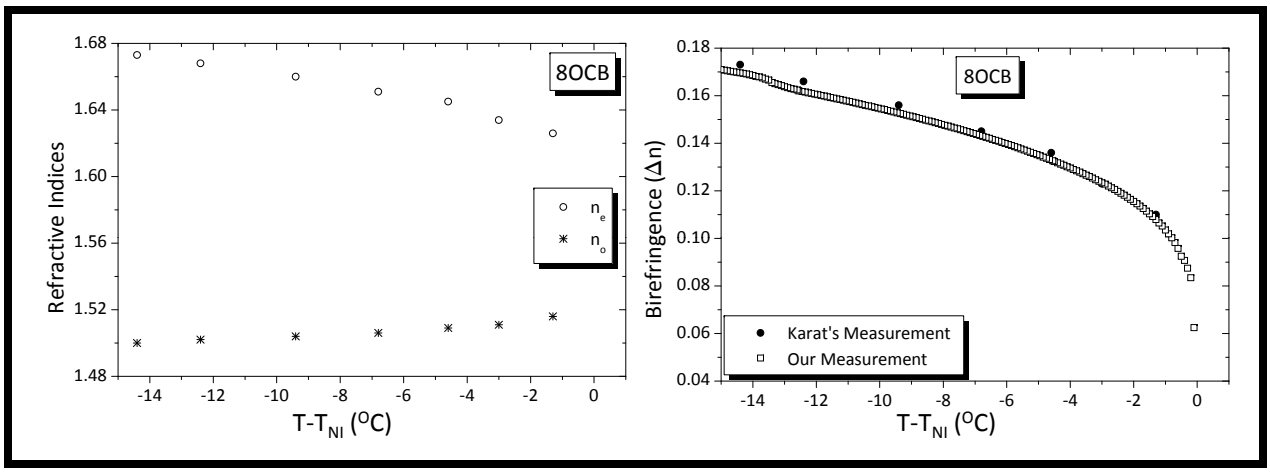

FIGURE 2.14: Ordinary and extra-ordinary refractive indices (λ =632.8nm) of 8OCB sample, measured by Karat[31]. $(n_e - n_o)$ of Karat's data is compared with our data. Both match well.

more sensitive to the accuracy of Δn than that of n_o. We have measured Δn very accurately (see Figure 2.11) and we assume that n_o has a fixed value of 1.5 at all temperatures. This assumption is used in all further calculations of K_{33}.

Figure 2.15 shows the splay elastic constants (K_{11}) at different temperatures. K_{11} increases monotonically with decrease in temperature. The data are compared with the earlier measurements from our laboratory by Karat *et al.* [31] which were later reanalyzed by Madhusudana *et al.* [32]. Our values are higher by $\sim$15%. This difference arises because in Karat's measurements using magnetic fields, the anisotropy of diamagnetic susceptibility ($\Delta\chi$) was calculated using an indirect method. The present result shows a smoother variation of K_{11} with temperature compared to the earlier data as the temperature stability is higher. The bend elastic constant (K_{33}) (see Figure 2.16) also shows a large pre-transitional divergence close to N-SmA transition point, as expected[1].

2.11 Conclusions

Thus the experimental setup that we have described in this chapter allows us to measure the birefringence Δn, the dielectric constants $\epsilon_\perp$, $\epsilon_\parallel$, the curvature elastic constants K_{11} and K_{33} using a *single sample cell* which has a planar orientation of the nematic director in materials with positive dielectric anisotropy $\Delta\epsilon$. Our data on 8OCB compare very well with earlier measurements,

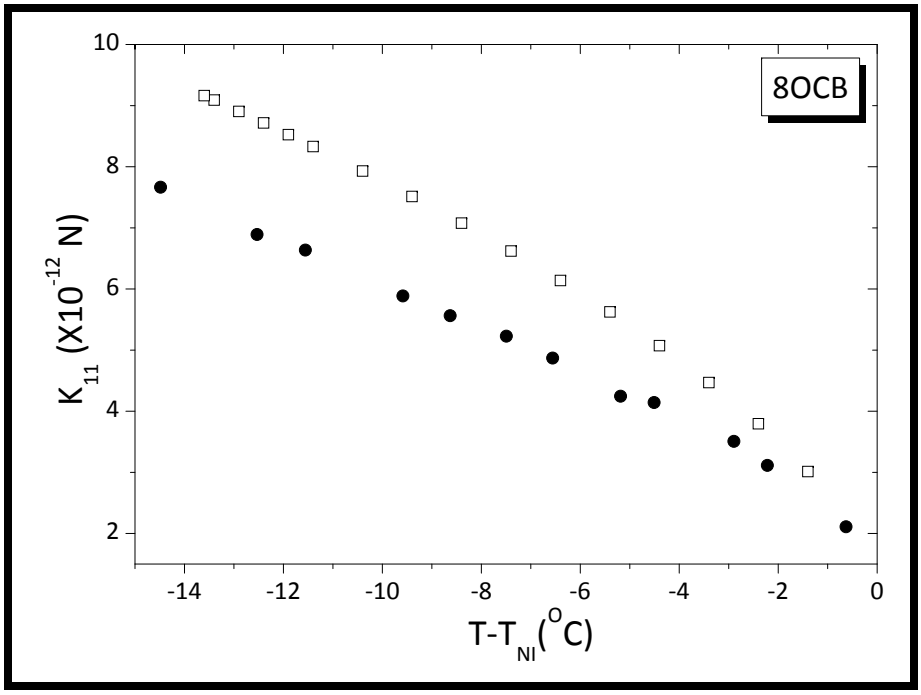

FIGURE 2.15: Measured values of splay elastic constants of 8OCB sample. □ represent our measurements and ● represent Karat's measurements[31] (later re-analyzed by Madhusudana and Pratibha[32])

as far as Δn is concerned. We believe that our measurements of $\epsilon_\perp$, $\epsilon_\parallel$, K_{11} and K_{33} are more accurate than the earlier measurements.

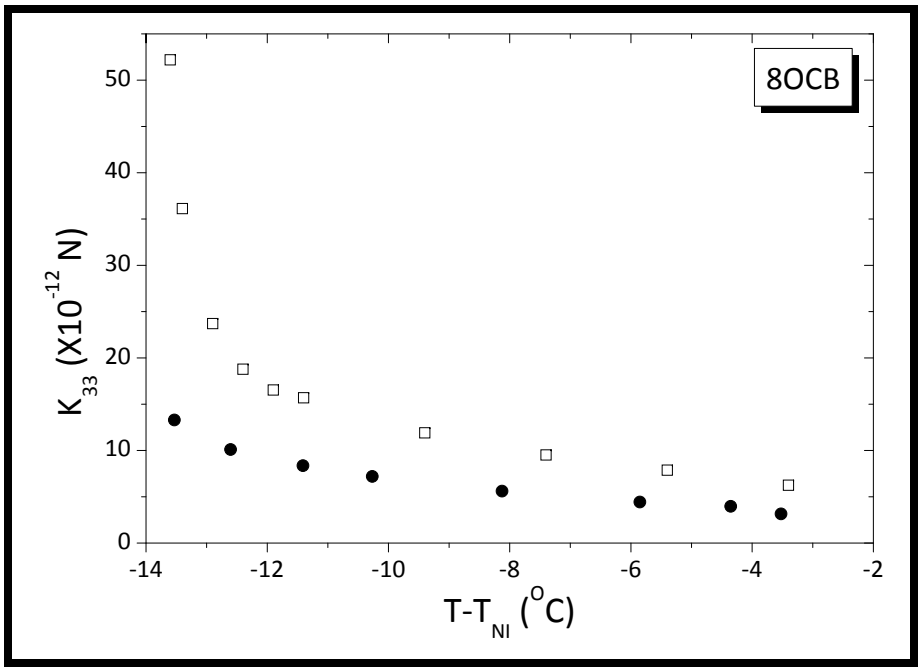

Figure 2.16: Measured values of bend elastic constants of 8OCB sample. □ represent our measurements and ● represent Karat's measurements[31] (later re-analyzed by Madhusudana and Pratibha[32])